crystals

MDPI

Article

Interplay of Isomorphs and Polymorphs of Amidino-Copper(II) Complexes with Different Halides

Zaina Yamba, Anna Peoble, Egor M. Novikov, Raúl Castañeda and Tatiana V. Timofeeva *

Department of Chemistry, New Mexico Highlands University, Las Vegas, NM 87701, USA; ademeyoyamba@live.nmhu.edu (Z.Y.); apeoble@live.nmhu.edu (A.P.); enovikov@live.nmhu.edu (E.M.N.); lrcastaneda@nmhu.edu (R.C.)

* Correspondence: tvtimofeeva@nmhu.edu

Abstract: To increase the number of potential materials for application as MRI contrast agents, several Cu(II) complexes were synthesized. Cu(II) complexes were chosen because they are less expensive in comparison with the presently used Gd(III), Mn(II) and other agents. Pyridine-2-carboximidamide (**1**), pyrimidine-2-carboximidamide (**2**) and pyrazole-2-carboximidamide (**3**) in the form of different salts along with $CuCl_2$ and NaCl or $CuBr^2$ and NaBr were used to obtain four Cu(II) complexes: dichloro-pyrimidine-2-carboximidamide copper(II) (**4**), dibromo-pyrimidine-2-carboximidamide copper(II) (**5**), dichloro-pirazole-2-carboximidamide copper(II) (**6**), and dibromo-pirazole-2-carboximidamide copper(II) (**7**). X-ray diffraction analysis revealed that molecular complexes **4**–**7** contain square planar coordinated Cu(II) atoms and their structures are very similar, as well as their packing in crystals, which allows us to consider them isomorphs. The same synthetic approach to complex preparation where NaCl or NaBr was not used brought us to the formation of dimeric complexes μ-chloro{chloro(pyridine-2-carboximidamide)copper(II)} (**8**) and μ-chloro{chloro(pyrimidine-2-carboximidamide)copper(II)} (**9**). In the dimeric complexes, two fragments which were the same as in monomeric complexes **4**–**7** are held together by bridging Cu-Cl bonds making the coordination of Cu equal to 5 (square pyramid). In dimeric complexes, axial Cu-Cl bonds are 2.7360 and 2.854 Å. These values are Cu-Cl bonds on the edge of existence according to statistical data from CSD. Synthesized complexes were characterized by IR spectroscopy, TGA, PXRD, EPR, and quantum chemical calculations. The higher thermal stability of monomer pyrimidine-based complexes with Cl and Br substituents makes them more prospective for further studies.

Keywords: isomorphs; polymorphs; Cu(II) complexes; EPR

Citation: Yamba, Z.; Peoble, A.; Novikov, E.M.; Castañeda, R.; Timofeeva, T.V. Interplay of Isomorphs and Polymorphs of Amidino-Copper(II) Complexes with Different Halides. *Crystals* **2024**, *14*, 319. https://doi.org/10.3390/cryst14040319

Academic Editor: Kil Sik Min

Received: 29 February 2024
Revised: 17 March 2024
Accepted: 25 March 2024
Published: 29 March 2024

1. Introduction

Research in magnetic resonance imaging (MRI) over the last forty years has developed into a large field, which includes explorations in different areas of science and clinical diagnosis [1–3]. The major reasons for this growth are its ionizing radiation-free nature and its capability to create 3D images of organisms [4]. For enhancing imaging accuracy and improving imaging, quality contrast agents are used [5]. Despite the widespread use of Gadolinium (III)-based agents, concerns have arisen regarding their toxicity, for instance, in patients with renal issues [6]. These concerns are linked to the thermodynamic instability and kinetic lability of these agents, prompting a search for safer MRI contrast agents capable of targeting specific organs and tumors while being safe for individuals with kidney disorders [6,7]. Despite the fact that Gd-based complexes are the main contrast MRI agents in clinical use, their potential toxicity provokes a search for contrast agents with alternative metal-ions such as Mn(II), Ln(III), and Fe clusters [8–12].

To increase the number of potential prototypes of pharmaceutical materials that can serve as imaging agents during MRI procedures, we synthesized and characterized several Cu(II) complexes with three ligands: pyridine-2-carboximidamide (**1**), pyrimidine-2-carboximidamide (**2**) and pyrazole-2-carboximidamide (**3**) (Schemes 1 and 2). As MRI

contrast agents, Cu(II) complexes are much less studied because of their low total spin (S = ½), but they bring unique opportunities, as Cu(II) can be reduced to a diamagnetic state, allowing building contrast agents that can be turned off and on. Antimicrobial and antiviral activities of pyridine, pyrimidine, and pyrazole derivatives are also discussed in the literature [13–15]. These prototype materials can help us to figure out possibilities of the formation of similar metal complexes with other metals utilizing ligands which we used in this study. It is known that such ligands can form different types of chelate complexes using active N atoms in heterocycles and carboximidamide groups [16]. In addition, two different halogens, Cl and Br, were used for complex formation. Corresponding to reaction conditions and reagents used for complex synthesis, the number and position of chelate ligands can differ, so it was important to support data on their structure using X-ray analysis. From the literature, it is known that, in many cases, variation of halogen in haloorganic crystals brings on the formation of isostructural crystals [17–23]. The existence of isostructural solids gives a serious lead to the search for materials (in our case pharmaceutical materials) with similar properties that allow us to find the best representatives in the series studied for further applications.

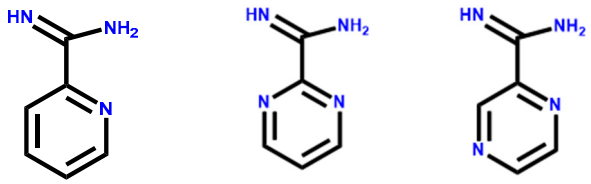

(**1**) (**2**) (**3**)

Scheme 1. Structure of ligands **1**–**3**.

Synthesized complexes with general Formulas (**4**)–(**9**) are shown below.

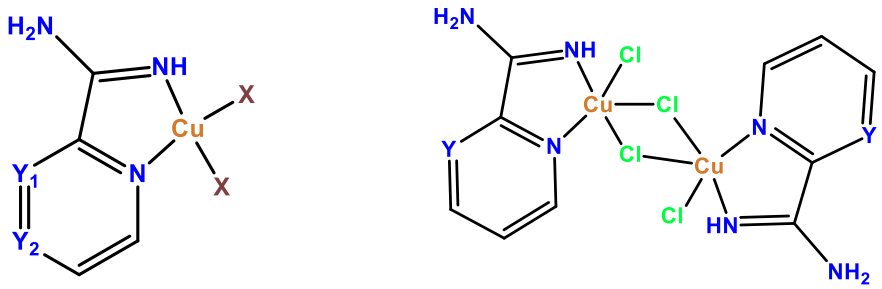

(**4**)–(**7**) (**8**)–(**9**)

Y_1 = N, Y_2 = CH, Hal = Cl (**4**) Y = CH (**8**)

Y_1 = N, Y_2 = CH, Hal = Br (**5**) Y = N (**9**)

Y_1 = CH, Y_2 = N, Hal = Cl (**6**)

Y_1 = CH, Y_2 = N, Hal = Br (**7**)

Scheme 2. Abbreviation for the complexes presented.

Several other methods such as IR spectroscopy, NMR, PXRD, TGA, EPR, and quantum chemical calculations were used for the characterization of obtained materials.

2. Materials and Methods

2.1. General

Most of the materials used for synthesis were purchased from commercial sources and used without further purification. Ligand **1** in the form of picolinimidamide hydrochlo-

ride salt was purchased from AMBEED. Ligand **2** was synthesized using the procedure described in [24], and ligand **3** was obtained using a similar procedure modified by us. As neutral molecules **2** and **3** naturally decompose, they were stabilized by making them trifluoroacetate salts. Complexes **4**–**9** were synthesized as described below.

IR spectra for all ligands and crystals were recorded using Pea rkin Elmer—Spectrum Two FT-IR Spectrophotometer (4000–450 cm^{-1}) loaded with Perkin Elmer UATR Two, featuring a diamond prism center for solid-state IR measurements. ^{1}H and ^{13}C NMR measurements were performed for $\mathbf{[2]^{+}[O_2C_2F_3]^{-}}$ and $\mathbf{[3]^{+}[O_2C_2F_3]^{-}}$ in DMSO-d_6 as well as ^{1}H NMR measurements were performed using Bruker b300 MHz and 75MHz spectrometer at 25 °C. TGA measurement for all crystals was performed using Hitachi STA7200 Thermal Analysis System loaded with N_2 gas and TGA Measure Software (TA7000 Standard Analysis, Version 10.1 Build 2001). EPR measurements were performed using Bruker EMXplus EPR Spectrometer with a Microwave Frequency Range (CW X-Band) of 9–9.8 GHz.

2.2. Synthesis of Pyrimidine-2-Carboximidamide Salt $\boldsymbol{[2]^{+}[O_2C_2F_3]^{-}}$

Synthesis of Pyrimidine-2-carboximidamide was performed following the synthetic procedure described by Safin et al. [24]. The salt was made by dissolving **2** (8.3399 mmol, 1018.3 mg) in 6 mL of a 1:1 ethanol to trifluoroacetic acid solution. A white crystalline precipitate started to form immediately. The product yield was 67% (1.2676 g). Decomposition temperature at 5% weight loss (TGA) was 215.3 °C. IR ν cm^{-1}: 3325 (m), 2989 (m), 1704 (s), 1668 (s), 1564 (s), 1538 (m), 1433 (m), 1404 (s), 1286 (w), 1239 (w), 1168 (s), 1118 (s), 1098 (s), 998 (m), 829 (s), 797 (s), 720 (s), 658 (s), 632 (s), 597 (m), 518 (m), 431 (s). ^{1}H-NMR (300 MHz, DMSO-d_6) δ: 9.92 (s, 1H), 9.70 (s, 1H), 9.15-9.13 (d, 2H), 7.93-7.90 (t, 1H). ^{1}H-NMR (300 MHz, D_2O) δ: 8.91 (d, 2H), 7.67 (t, 1H) ^{13}C-NMR (75 MHz, DMSO-d_6) δ: 125.29, 153.34, 158.78, 160.17.

2.3. Synthesis of Pyrazine-2-Carboximidamide Salt $\boldsymbol{[3]^{+}[O_2C_2F_3]^{-}}$

Synthesis of pyrazine-2-carboximidamide salt $\mathbf{[3]^{+}[O_2C_2F_3]^{-}}$ was performed using the following procedure similar to the synthetic procedure described by Safin et al. [24]. Cyanopyrazine purchased from TOKYO CHEMICAL INDUSTRY Co., Ltd. 6-15-9 TOSHIMA, KITA-KU, TOKYO, JAPAN (55.8516 mmol, 5870.0 mg) was dissolved in 50 mL of acetonitrile while stirring for 30 s in a 125 mL pressure vessel. The pressure vessel containing the mixture was placed in an ice bath and ammonia gas bubbled in the vessel for 10 min. The pressure vessel was tightly sealed and placed in an oil bath at 110 °C for 3 days. A ground coffee-colored product was obtained with a crude yield of 5.3322 g. The crude product (2239.7 mg) was dissolved in 16 mL of ethanol while stirring in a 50 mL Erlenmeyer flask. Trifluoroacetic acid (16 mL) was slowly added into the solution and the flask was capped and allowed to react for one day. Colorless needles were obtained the next day and filtered out and rinsed with ethanol. The product yield was 2.0035 g (8.52 mmol, 67%). Decomposition at 5% weight loss (TGA) was 212.3 °C. IR ν cm^{-1}: 3281 (w), 3021 (m), 1663 (s), 1580 (w), 1525 (m), 1461 (m), 1442 (m), 1405 (m), 1191 (s), 1134 (s), 1041 (w), 1017 (s), 873 (m), 843 (s), 797 (s), 759 (s), 774 (m), 722 (s), 515 (w), 425 (s). ^{1}H-NMR (300 MHz, DMSO-d_6) δ 9.68 (s, 2H), 9.39-9.38 (d, 2H), 9.05-9.04 (d, 1H), 8.94-8.93 (dd, 1H). ^{13}C-NMR (75 MHz, DMSO-d_6) δ: 141.04, 144.56, 145.00, 149.65, 161.54.

2.4. Synthesis of Complex ***4***

The salt of ligand **2** $\mathbf{[2]^{+}[O_2C_2F_3]^{-}}$ (2.263 mmol, 534.8 mg) was dissolved in 4 mL of methanol. In a separate vial, copper(II) chloride dihydrate (2.263 mmol, 386.70 mg) was dissolved in 5 mL of a saturated NaCl methanol solution. The copper(II) chloride solution was filtered on top of the ligand solution, and crystallization began immediately. Ligand's molar ratio to $CuCl_2$ was 1:1. The mixture was sealed with parafilm and crystallized for one day. The greenish-brownish crystals were filtered out, rinsed with isopropanol, and weighed. After filtration, the product yield was 430.9 mg (1.68 mmol, 74%). Decomposition

at 5% weight loss (TGA) was 266.0 °C. IR ν cm^{-1}: 3382 (m), 3255 (m), 1652 (s), 1583 (s), 1563 (s), 1506 (m), 1448 (w), 1406 (s), 1246 (w), 1197 (w), 1131 (w), 1061 (w), 1020 (w), 828 (m), 816 (s), 793 (s), 698 (w), 672 (w), 655 (s), 643 (m), 575 (s), 477 (w).

*2.5. Synthesis of Complex **5***

The salt of ligand **2** $\mathbf{[2]^+[O_2C_2F_3]^-}$ (1.271 mmol, 300.1 mg) was dissolved in 4 mL of methanol. In a separate vial, copper(II) bromide, $CuBr_2$ (1.271 mmol, 284.0 mg) was dissolved in 4 mL of a saturated NaBr methanol solution. The copper(II) bromide solution was filtered on top of the ligand solution, and crystals began to form immediately and after one-day crystallization was completed. The ligand's molar ratio to $CuBr_2$ was 1:1. The mixture was sealed with parafilm and allowed to crystallize for one day. The greenish-brownish crystals were filtered out, rinsed with isopropanol, and weighed. The product yield after filtration was 343 mg (0.99 mmol, 78%). Decomposition at 5% weight loss (TGA) was 262.7 °C. IR ν cm^{-1}: 3373 (m), 3253 (m), 1654 (s), 1580 (s), 1565 (m), 1500 (m), 1405 (s), 1245 (w), 1193 (w), 1125 (w), 1078 (w), 1058 (s), 1017 (w), 817 (s), 788 (s), 683 (w), 672 (w), 654 (s), 639 (m), 561 (s), 476 (w).

*2.6. Synthesis of Complex **6***

The salt of ligand **3** $\mathbf{[3]^+[O_2C_2F_3]^-}$ (0.212 mmol, 50.1 mg) was dissolved in 2 mL of methanol. In a separate vial, copper(II) chloride dihydrate (0.212 mmol, 37.10 mg) was dissolved in 2 mL of a saturated NaCl methanol solution. The copper(II) chloride solution was filtered on top of the ligand solution, and crystals began to form immediately. Ligand's molar ratio to $CuCl_2$ was 1:1. The mixture was sealed with parafilm and allowed to crystallize for a day. The greenish-brownish crystals were filtered out, rinsed with isopropanol, and weighed. The product yield after filtration was 49.1 mg (0.19 mmol, 60%). Decomposition at 5% weight loss (TGA) was 199.5 °C; IR ν cm^{-1}: 3361 (w), 3289 (w), 1648 (s), 1570 (m), 1534 (w), 1501 (w), 1451 (s), 1399 (s), 1304 (w), 1237 (w), 1190 (w), 1073 (w), 1048 (m), 1037 (s), 860 (m), 816 (s), 764 (m), 681 (w), 627 (w), 544 (s), 482 (m), 450 (s).

*2.7. Synthesis of Complex **7***

The salt of ligand **3** $\mathbf{[3]^+[O_2C_2F_3]^-}$ (0.212 mmol, 50.1 mg) was dissolved in 2 mL of methanol. In a separate vial, copper(II) bromide (0.212 mmol, 47.30 mg) was dissolved in 2 mL of a saturated NaBr methanol solution. The copper(II) bromide solution was filtered on top of the ligand solution, and crystals began to form immediately, and after one-day crystallization was completed. Ligand's molar ratio to $CuBr_2$ was 1:1. The mixture was sealed with parafilm and allowed to crystallize for a day. The greenish-brownish crystals formed were filtered out, rinsed with isopropanol, and weighed. The product yield after filtration was 63.6 mg (018 mmol, 58%). Decomposition at 5% weight loss (TGA) was 238.2 °C. IR ν cm^{-1}: 3366 (w), 3270 (w), 1645 (s), 1567 (m), 1531 (w), 1497 (w), 1447 (m), 1397 (m), 1302 (w), 1229 (w), 1172 (w), 1067 (w), 1049 (w), 1035 (m), 859 (w), 802 (m), 798 (m), 762 (m), 677 (w), 609 (w), 478 (s), 444 (s).

*2.8. Synthesis of Complex **8***

The reaction was conducted under atmospheric conditions. In separate vials, pyridine-2-amidine hydrochloride (0.1460 g, 0.92 mmol) and copper(II) chloride dihydrate (0.1579 g; 0.92 mmol) were dissolved using 6 mL and 5 mL of methanol, respectively. Then both solutions were combined, and the flask was capped with a rubber stopper. The green crystals formed were filtered out, rinsed with isopropanol, and weighed. The product yield after filtration was 0.1771 g (0.69 mmol, 75%). Decomposition (weight loss) by TGA was 361.7 °C IR ν cm^{-1}: 3373 (m), 3326 (w), 3278 (m), 3215 (w), 3195 (w), 1656 (s), 1585 (m), 1570 (m), 1506 (w), 1451 (s), 1437 (m), 1304 (m), 1275 (w), 1238 (m), 1196 (w), 1177 (w), 1160 (w), 1115 (w), 1080 (w), 1053 (w), 1020 (s), 900 (m), 821 (s), 795 (s), 747 (s), 680 (w), 663 (w), 643 (m), 571 (m), 535 (s), 506 (s).

2.9. Synthesis of **9**

The ligand **2** (0.371 mmol, 44.50 mg) was dissolved in 3 mL of dichloromethane. In a separate vial copper(II) chloride dihydrate (0.371 mmol, 63.7 mg) was dissolved in 3 mL of methanol. The copper(II) chloride solution was filtered on top of the ligand solution. Ligand's molar ratio to $CuCl_2$ was 1:1. The resultant solution was placed in a vial, sealed with parafilm, and allowed to crystallize. After one day the green crystals were formed, filtered out, rinsed with isopropanol, and weighed. The product yield after filtration was 47.1 mg (0.09 mmol, 50%. Decomposition at 5% weight loss (TGA) was 226.0 °C. IR ν cm^{-1}: 3378 (m), 3279 (m), 1658 (s), 1581 (s), 1502 (w), 1440 (w), 1400 (s), 1242 (m), 1199 (w), 1118 (w), 1063 (w), 1017 (m), 829 (s), 801 (m), 679 (w), 652 (s), 578 (s), 538 (s), 476 (m), 426 (w).

2.10. X-ray Structure Analysis

Single-crystal XRD data of **5** and **7** were collected using Rigaku XtaLAB Synergy (Dualflex): HyPix 6000, rail XtaLab Synergy Standard with CuKα (λ = 1.54184) at 100 K. Absorption correction was applied using the Gaussian technique. The structure was solved and refined with ShelXT and ShelXL [25] refinement packages. Single-crystal XRD data collection of **[2]$^+$[$O_2C_2F_3$]$^-$**, **4**, **6**, **8** and **9** was performed on a Bruker Smart APEX-II CCD diffractometer with MoKα (λ = 0.71073) at 100 K temperature. The absorption correction was performed by a multi-scan method using SADABS-2016/2 (Bruker, Madison, WI, USA, 2016/2). The diffraction measurement method was ϕ and ω-scans. The structures were solved with the ShelXT [25] and refined with the ShelXL [25] refinement package. In complex 7 positions of H atoms in amino group N(4) were found to be disordered, located above and below the plane of symmetry and their positions were refined with 50% probability. Important details of X-ray data collection and structure solution are presented in Table 1 (complexes **4**–**9**) and Table S1 (ligand **[2]$^+$[$O_2C_2F_3$]$^-$**).

Table 1. Crystallographic data collection and refinement for **4**–**9**.

	4	**5**	**6**	**7**	**8**	**9**
Formula	$C_5H_6Cl_2CuN_4$	$C_5H_6Br_2CuN_4$	$C_5H_6Cl_2CuN_4$	$C_5H_6Br_2CuN_4$	$C_{12}H_{14}Cl_4Cu_2N_6$	$C_{10}H_{12}Cl_4Cu_2N_8$
Formula weight	256.58	345.484	256.58	345.50	255.59	256.581
Temperature/K	100	100	100	100	100	100
Crystal system	Orthorhombic	Orthorhombic	Orthorhombic	Orthorhombic	Monoclinic	Monoclinic
Space group, Z	Pnma, 4	Pnma, 4	Pnma, 4	Pnma, 4	$P2_1/n$, 4	$P2_1/n$, 4
a/Å	8.710 (6)	8.924 (2)	8.6664 (2)	8.98 (5)	8.3731 (4)	8.4622 (12)
b/Å	6.292 (5)	6.3937 (16)	6.2964 (2)	6.43 (3)	10.9315 (6)	10.6392 (14)
c/Å	15.260 (11)	15.626 (4)	14.8940 (4)	15.22 (14)	9.5637 (3)	9.6678 (13)
α/°	90	90	90	90	90	90
β/°	90	90	90	90	103.022 (4)	99.036 (5)
γ/°	90	90	90	90	90	90
Volume/Å^3	836.4 (11)	891.5 (4)	812.72 (4)	879 (11)	852.86 (7)	859.6 (2)
ρ_{calc}g/cm^3	2.038	2.574	2.097	2.610	1.991	1.983
μ/mm^{-1}	3.193	11.359	9.398	13.745	3.127	3.106
F(000)	508.0	652.1	508.0	652.0	508.0	508.0
Crystal size/mm^3	0.3 × 0.09 × 0.04	0.4 × 0.15 × 0.05	0.06 × 0.03 × 0.01	0.05 × 0.02 × 0.01	0.5 × 0.25 × 0.15	0.4 × 0.15 × 0.15

Table 1. *Cont.*

	4	**5**	**6**	**7**	**8**	**9**
Radiation	Mo Kα (λ = 0.71073)	Mo Kα (λ = 0.71073)	Cu Kα (λ = 1.54184)	Cu Kα (λ = 1.54184)	Mo Kα (λ = 0.71073)	Mo Kα (λ = 0.71073)
Reflections Collected	17,318	11,741	7265	4587	7902	16,659
Independent Reflections	1376	1167	817	954	2956	2610
R_{int}	0.0488	0.0522	0.0455	0.0296	0.0463	0.0327
Data/parameters	1376/73	1167/82	817/75	954/76	2956/121	2610/121
Goodness-of-fit on F^2	1.344	1.073	1.103	1.049	1.050	1.017
R_1 [$I \geq 2\sigma$ (I)]	0.0697	0.0328	0.0604	0.0574	0.0420	0.0269
wR_2 [$I \geq 2\sigma$ (I)]	0.1601	0.0811	0.1548	0.1527	0.0889	0.0674
R_1 [all data]	0.0767	0.0440	0.0658	0.0602	0.0560	0.0343

Powder XRD analysis for all crystals was conducted using a Rigaku Ultima IV diffractometer equipped with Bragg–Brentano HD optics and Cu Kα radiation. All the complexes were placed in a flat sample holder for measurements.

Quantum chemical calculations of complex **4** were carried out with GAUSSIAN 16 software [26,27]. Geometry parameters and electronic properties were by using the DFT method at the B3LYP level of theory with 6–31(d) basis set. Starting molecular geometry was adopted from the results of X-ray diffraction analysis and fully optimized using the above-mentioned DFT approach which was successfully used before for Cu(II) complexes [27].

3. Results and Discussion

3.1. Crystal Structure of Ligand

The crystal structure of synthesized trifluoracetic acid (TFA) salts of ligand **2** was studied using single-crystal X-ray diffraction. Crystallography data for crystal $\mathbf{[2]^+[O_2C_2F_3]^-}$ are presented in Table S1. Ligand **2** and TFA in crystal form dimers with two hydrogen bonds N-H. . .O (Figure S1), which in turn form molecular ribbons with the same type of H-bonds (Figure S2).

3.2. Crystal Structure of Complexes

Depending on complex structures (organic ligands and halogens), the shape and color of crystals are different. Figure 1 demonstrates these differences for **4**–**7**, which are most probably related to absorption bands of Cu-Hal bonds. IR spectra of complexes **4**–**7** are alike (Figures S3–S6) which suggests that their molecular structures are also similar. This observation is supported by X-ray diffraction data which indicate the similarity of molecular and crystal structures of complexes **4**–**7**.

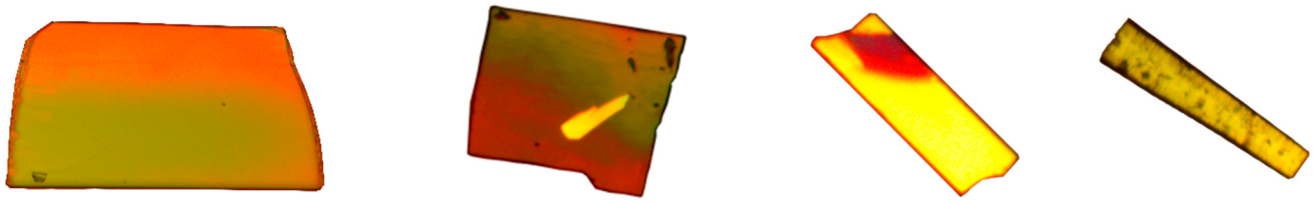

(**a**) (**b**) (**c**) (**d**)

Figure 1. Microscopic images of complexes **4**–**7**: (**a**) plate-like crystal **4**; (**b**) plate-like crystal **5**; (**c**) plate-like crystal **6**; (**d**) plate-like crystal **7**.

It should be mentioned that synthetic procedures to obtain these complexes were the same. For complexes **4**–**7**, the ligands were brought into reaction in the form of trifluoroacetic acid salt, and Hal anions in the form of $CuHal_2$ and NaHal salts (Hal = Cl, Br). X-ray data for complexes **4**–**7** demonstrated not only the same molecular structure for all these complexes (Figure 2) but also the same molecular packing in the crystal which allows us to consider these crystals isomorphic.

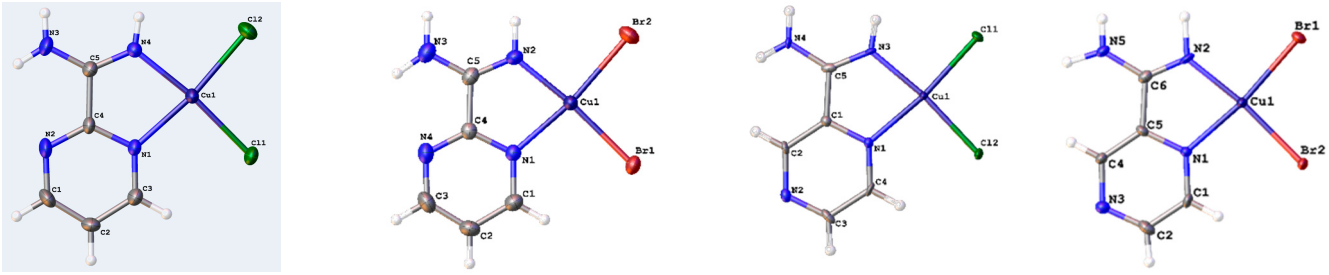

(**a**) (**b**) (**c**) (**d**)

Figure 2. Molecular structure of complexes **4** (**a**), **5** (**b**), **6** (**c**), and **7** (**d**) in crystal with thermal ellipsoids 50% probability.

Selected geometry parameters of the complexes **4**–**9** are presented in Table 2. Usually, Cu(II), with a d^9 electron configuration, has square planar or octahedral geometry. In our case, complexes of Cu(II) have square planar coordination. It is possible to see (Table 2) that the coordination of Cu-N distances in complexes **4**–**7** vary insignificantly with different halogen Cl and Br ligands and with different **2** and **3** ligands. Distance Cu-Hal corresponds to the average values of such bonds. All molecules in the crystal lattice are planar since they are located on crystallographic mirror planes. The sum of bond angles around Cu atoms is equal to 360°.

Table 2. Selected bond lengths and bond angles in complexes **4**–**9**.

	Complexes					
Bond, Å	**4**	**5**	**6**	**7**	**8**	**9**
Cu1-N1	2.058 (7)	2.062 (4)	1.950 (5)	2.071 (15)	2.045 (2)	2.0607 (15)
Cu1-N2	1.973 (7)	1.951 (5)	2.050 (6)	1.958 (12)	1.949 (2)	1.9504 (15)
Cu1-Hal2	2.283 (3)	2.4307 (10)	2.2570 (2)	2.403 (17)	2.2745 (7)	2.2520 (6)
Cu1-Hal1	2.249 (3)	2.3874 (9)	2.2578 (18)	2.396 (12)	2.2747 (7)	2.2540 (5)
Cu1-Hal3					2.7360 (7)	2.854 (6)
Angle, degr.						
N1-Cu1-N4	80.62 (3)	80.44 (19)	79.9 (2)	79.2 (6)	80.14 (9)	79.99 (6)
N1-Cu1-Hal1	92.84 (2)	93.99 (13)	93.28 (16)	94.4 (6)	94.83 (6)	93.85 (4)
N4-Cu1-Hal2	91.70 (2)	91.47 (14)	92.87 (17)	93.2 (6)	90.90 (7)	91.10 (5)
Hal1-Cu1-Hal2	94.84 (11)	94.10 (4)	93.94 (7)	93.2 (6)	92.61 (3)	94.23 (19)
Hal1-Cu1-Hal3					91.86 (2)	92.987 (18)
Hal2-Cu1-Hal3					101.08 (3)	106.225 (18)
N1-Cu1-Hal3					92.85 (6)	84.73 (4)
N2-Cu1-Hal3					94.15 (7)	90.09 (5)

In crystals **4**–**7**, planar molecules are packed in antiparallel layers along axis *b*. Due to molecular positions on mirror planes, distances between such layers are equal to *b*/2 (3.146 (5), 3.1968 (16), 3.1482 (2), 3.22 (3) Å for **4**–**7**, respectively), suggesting significant intermolecular interactions between complexes in different layers. Relative positions of the closest molecules from neighboring layers are demonstrated in Figure 3b,c for complexes **4** and **6**, and in Table 3 for complexes **4**–**7**.

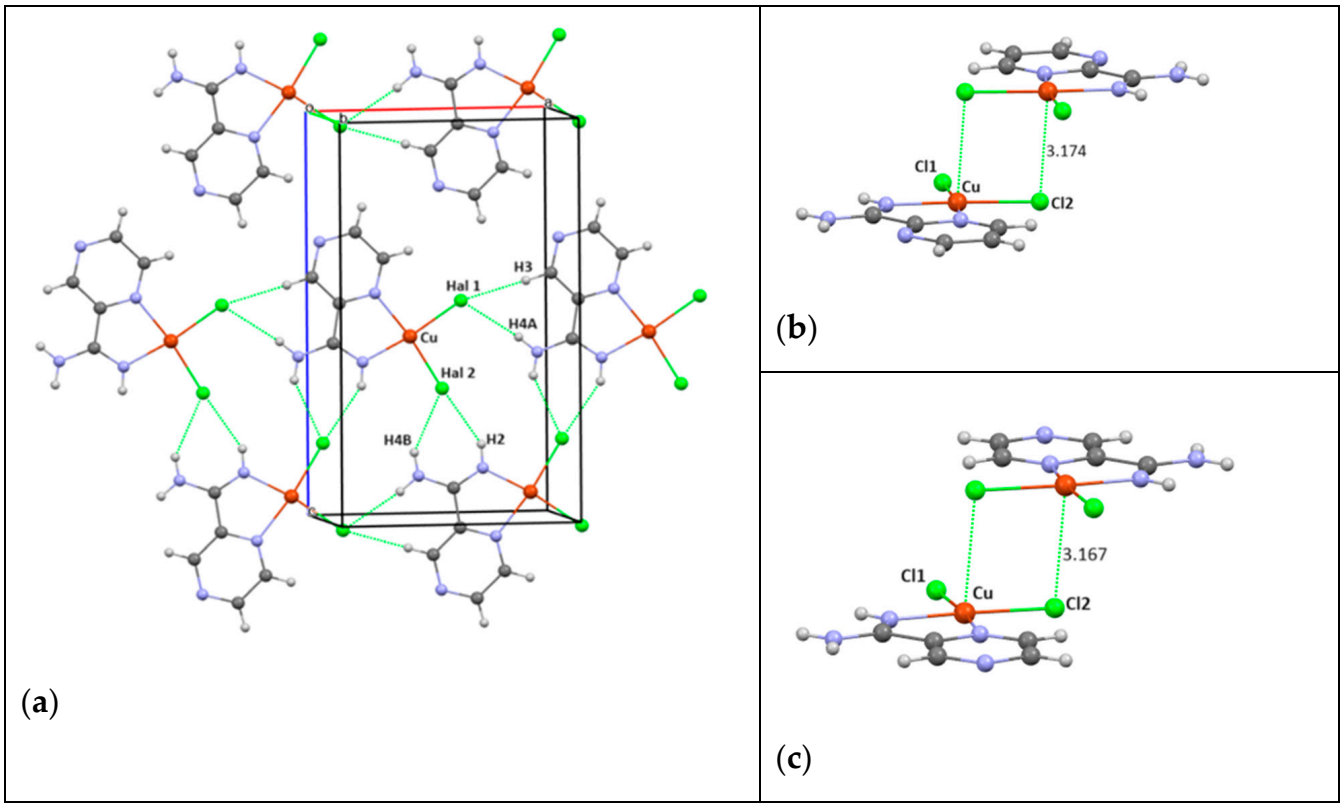

Figure 3. (**a**) Scheme of packing in molecular layers in isomorphic structures **4**–**7**. Short intermolecular contacts Cl. . .H are shown with green dotted lines. (**b**) Scheme of molecular positions of complexes **4** from different layers, demonstrating that axial position at Cu atom is taken by Cl atom from complex in neighboring molecular layer. (**c**) Same scheme for complex **6**.

Table 3. Short intermolecular contacts with Halogen atoms in crystal structures **4**–**7**.

Contact, Å	**Structure**			
In Layer	**4/Cl**	**5/Br**	**6/Cl**	**7/Br**
Hal1. . .H3 (B)	2.612 (3)	2.629 (5)	2.459 (13)	2.589 (8)
Hal1. . .H4A	-	-	2.501 (16)	Disordered H
Hal2. . .H2	2.537 (3)	2.561 (6)	2.517 (15)	2.580 (5)
Hal2. . .H4B(A)	2.615 (3)	2.615 (6)	2.560 (15)	Disordered H
Between Layers				
Cu. . .Hal *	3.174 (3)	3.210 (8)	3.167 (3)	3.223 (14)

* See these contacts in Figure 3b,c.

The general presentation of molecular positions in layers in crystals **4**–**7** is shown in Figure 3a. The structure of this layer is defined by short contacts of Cl. . .H type (Table 3) which are shorter than the sum of van der Waals radii of Cl/Br and H atoms by approximately 0.3–0.5 Å [28] depending on which van der Waals radii system is used. The simple explanation of such short contacts is electrostatic interactions between positively

charged H and negatively charged Cl atoms (see Figure S10). It should be mentioned that in these structures it is possible to observe relatively short contacts between complexes in molecular layers. In Figure 3b,c, molecules from different layers connected by inversion center are presented. For these molecules, it is possible to speculate that Cu atoms have a trend to increase their coordination number from 4 to 5 by including into their coordination sphere additional Cl atoms from neighboring molecules and forming a square-pyramidal environment with long axial metal–ligand distance. Distances between Cu and Cl at the vertex of the square pyramid are shown in Figure 3 for molecules **4** and **6** and for molecules **4**–**7** in Table 3.

Complexes **8** and **9** were synthesized by using slightly different procedures from complexes **4**–**7**; namely, in both reactions, sodium chloride was not added. The green rod-like complexes **8** and **9** (Figure 4) are significantly different from plate-like yellow-brownish complexes **4**–**7**. Since complexes **4** and **9** were obtained with ligand **2** and $CuCl_2$, it gave the possibility to speculate that these materials are polymorphs. However, X-ray analysis of complexes **8** and **9** indicated that both these complexes are dimers connected by two long bridging bonds Cu-Cl in the axial position to the square coordination plane of Cu. Differences in IR solution spectra of complexes **4** and **9** (Figure S9) formed with ligand **2**, which allows us to suggest that we are dealing with true dimers, not with just specific molecular orientations in crystals caused by antiparallel orientations of molecular dipole moments (see Figure 3b,c). So, in the case of a lower concentration of Cl^- anions in the reaction mixture, dimeric complexes with pentacoordinated Cu(II) were obtained (Figure 5). It should be mentioned that Cu(II) was called, in the literature, a "chameleon" in coordination chemistry since it can have 4, 5, and 6 coordination numbers depending on ligand types and reaction conditions [29]. For 5-coordinated Cu(II) trigonal bipyramidal and square pyramidal coordination are common. In the case of complexes **4**–**7**, restrictions imposed by polydentate ligands resulted in the formation of planar square Cu(II) coordination, and square pyramidal coordination for complexes **8** and **9** (Figure 5) with Cu-Cl(axial) distances 2.738 (7) and 2.854 (6) Å, respectively. If, in the complexes **4**–**7**, the Cu atom lays in the same plane as all ligands forming square planar Cu surrounding, in molecules **8** and **9**, Cu atoms are located slightly above the coordination plane of four kay ligand's atoms by 0.150 (7) and 0.144 (4) Å, respectively.

(**a**) (**b**)

Figure 4. Microscopic images of green rod-like crystals of complexes **8** (**a**) and **9** (**b**).

To find out if dimeric complexes **8** and **9** have coordination distances that are inside the range of similar Cu-Cl distances in complexes presented in CSD, a statistical analysis of such bonds was carried out. The histogram for Cu-Cl bonds is shown in Figure 6. It demonstrates a total of 1046 of such bonds in interval 2.74–2.93 Å as in **8** and **9**, but no such bonds above 3.1 Å as in **4**–**7**.

Unit cell parameters and molecular packing in crystals **8** and **9** demonstrate that these complexes are isostructural. Molecules in crystals **8** and **9** form ladder-like chains held together by π-staking interactions between heterocyclic fragments of their molecules (Figure 7) with distances between ligands mean planes 2.743 (9) and 3.026 (3) Å, respectively.

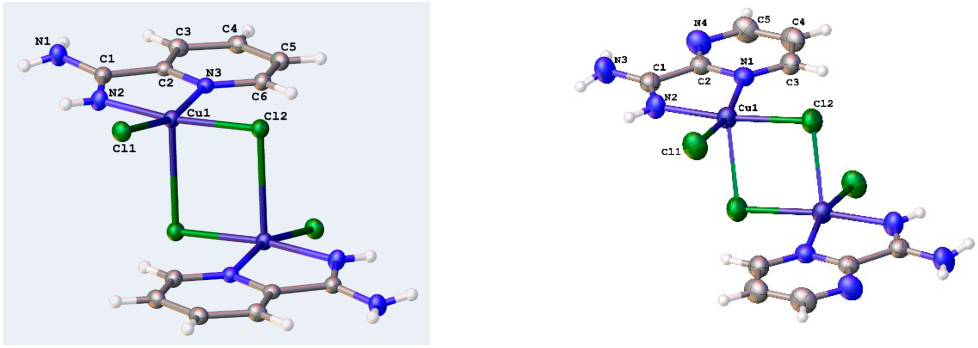

(**a**) (**b**)

Figure 5. The molecular structure of complexes **8** (**a**) and **9** (**b**) in crystal with thermal ellipsoids 50% probability.

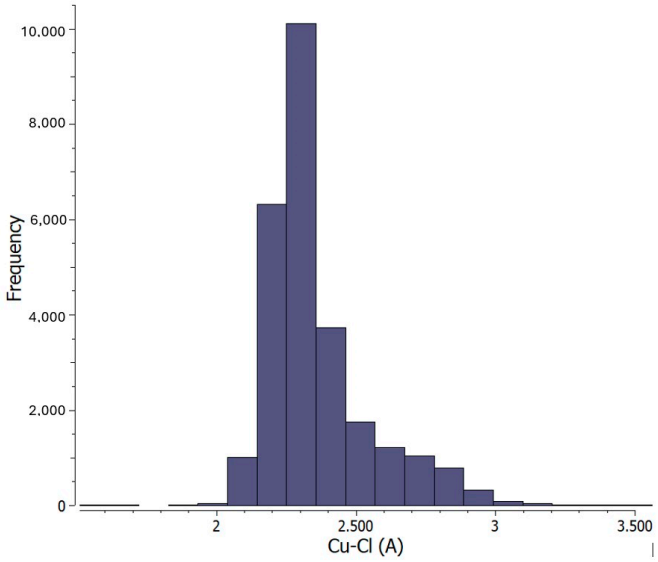

Figure 6. Histogram of Cu-Cl distances (Å) from CSD. A CSD search was conducted for all the structures with a Cu-Cl bond, with the only parameter used being the Cu-Cl distance. The search included all the oxidation states of copper, and the coordination number was not restricted. None of the elements were excluded from the search, so the search included ligands with atoms other than nitrogen. The version of the CSD used was 2023.1.

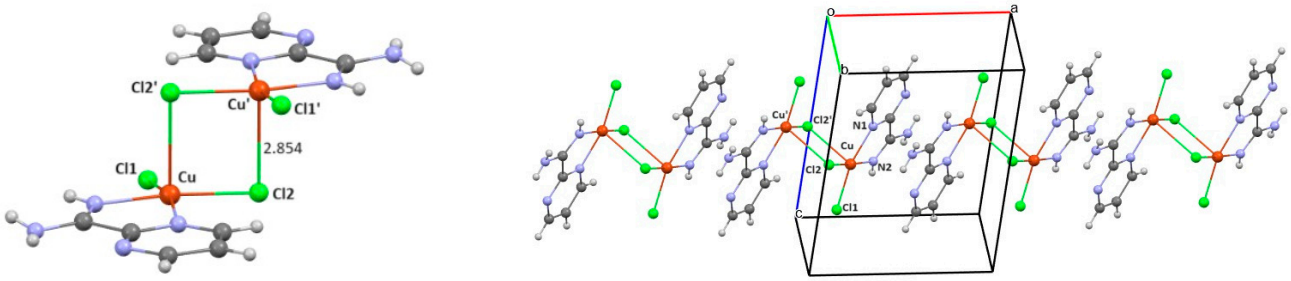

(**a**) (**b**)

Figure 7. Molecular structure of dimeric complex **9** (**a**) and molecular packing in crystal **9** (**b**).

The thermal stability of the synthesized complexes was characterized by decomposition temperature. From the data in Table 4, it is possible to see that the most stable complex is a complex **8** with ligand **1**. The complexes with ligand **2** are more stable than complexes with ligand **3**. However, complexes with ligand **2** have approximately the same stability with Cl and Br ligands, while for complexes with ligand **3**, stability with Br ligands is higher.

Table 4. The decomposition temperature of complexes **4**–**7** and **9**.

Complex	Ligands	Temperature, °C
4	**2, Cl**	266
5	**2, Br**	263
6	**3, Cl**	199.5
7	**3, Br**	238
8	**1, Cl**	362
9	**2, Cl**	226

To explore the possibility of the practical application of synthesized complexes as contrast agents for MRI, electron paramagnetic resonance (EPR) analysis was conducted on the solid-state samples of complexes **4** and **5**. Additionally, complexes **4** and **5** were soluble and stable in a PBS buffer with physiological pH, showing the opportunity to apply **4** and **5** as MRI contrast agents. On the other hand, **6** and **7** were not soluble in PBS buffer so they are not soluble in physiological conditions, as they precipitated and the blue solution disappeared. To better understand the magnetic behavior of **4** and **5**, we used PHI [30] to simulate the EPR of **4** and **5** at frequencies of 9.831 GHz for **4** and 9.868 GHz for **5** to delve into the magnetic properties of these complexes. The consideration of anisotropic and/or isotropic systems was essential, as these terms describe the magnetic interactions experienced by unpaired electrons in a paramagnetic sample. In isotropic systems, the magnetic properties are uniform, while in anisotropic systems, these properties are direction-dependent [31]. Given the distinct shapes of our complexes, anisotropic systems were chosen for the simulations. For complex **4**, the g_x, g_y, and g_z values were determined as 2.247, 2.054, and 2.031, respectively. On the other hand, the g_x, g_y, and g_z values for **5** were found to be 2.207, 2.049, and 2.049, respectively. The simulation calculated for each complex, referred to as **4 RES** and **5 RES**, was then compared with the experimental data (**4 EXP** and **5 EXP**). In the case of complex **5**, a notable correlation was observed between the simulated and experimental plots, showcasing close alignment with a few outliers (Figure 8). Conversely, for complex **4**, while some points exhibited similarity between the two plots, a larger number of outliers were identified (Figure 9). The discrepancies observed in the plots point to distinctive effects arising from the varied molecular behavior and magnetic properties exhibited by the complexes. The chemical environment of **4** and **5** is undoubtedly influenced by the presence of Chlorine and Bromine atoms within the complexes changing their respective EPR spectra.

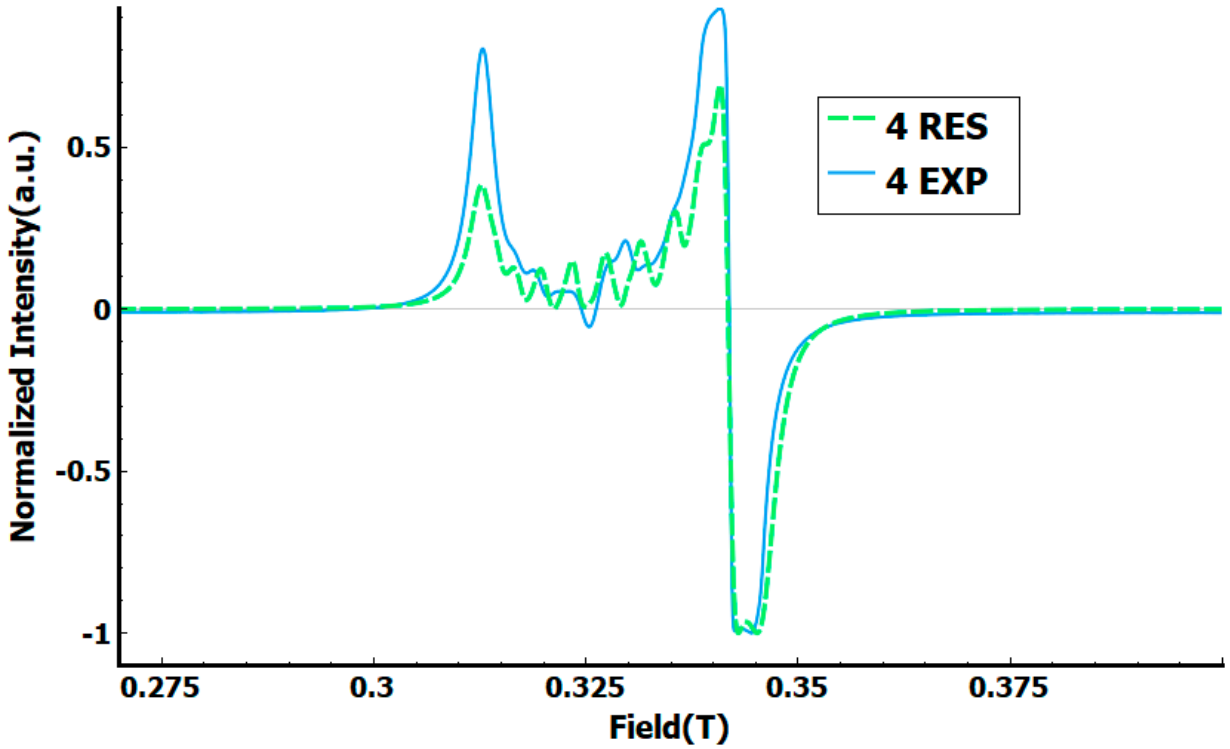

Figure 8. EPR plots of complex **4**: calculated (RES) and experimental (EXP).

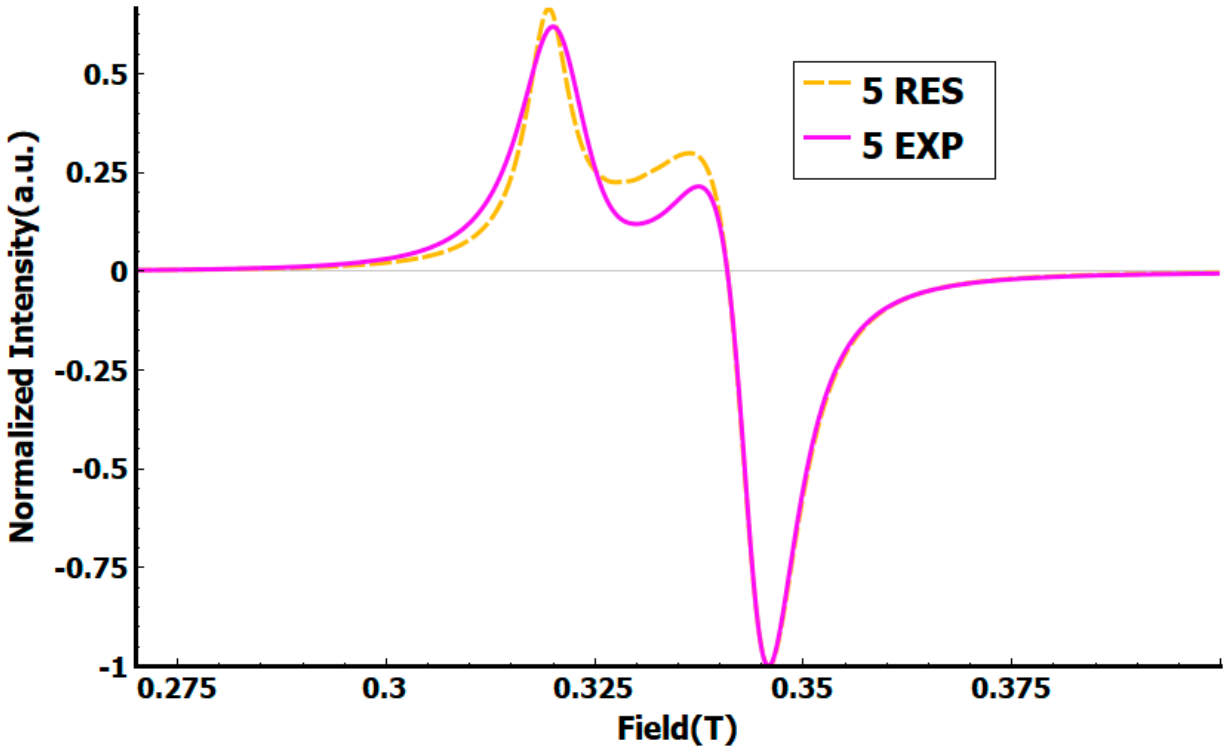

Figure 9. EPR plots of complex **5**: calculated (RES) and experimental (EXP).

4. Conclusions

Six Cu(II) complexes, namely dichloro(pyrimidine-2-carboximidamide)copper(II) (**4**), dibromo(pyrimidine-2-carboximidamide)copper(II) (**5**), dichloro(pirazole-2-carboximidamide) copper(II) (**6**), dibromo(pirazole-2-carboximidamide)copper(II) (**7**), μ-chloro{chloro(pyridine-2-carboximidamide)copper(II)} (**8**) and μ-chloro{chloro(pyrimidine-2-carboximidamide)copper

(II)} (**9**), were synthesized in high yields and characterized using several different methods such as IR spectroscopy, PXRD, TGA, EPR, and quantum chemical calculations. Complexes were crystallized, and their structures were established by single-crystal diffraction. Cu(II) in complexes **4**–**7** has square planar coordination, planar molecules have very similar structures and crystal packing, which allows us to call these crystals isostructural. Complexes **8** and **9** have a dimeric structure where two monomer-like fragments are bridged by Cu-Cl bonds, resulting in square pyramidal coordination for the Cu(II) ion and a similar herringbone packing motif. Likewise, **8** and **9** are isostructural despite having a different number of nitrogen atoms. It was found that the thermal stability of pyrimidine complexes (**4**, **5**) with Cl and Br ligands is higher than the stability of pyrazole complexes (**6**, **7**). Additionally, complexes **4**, **5** and **8** are soluble in a PBS buffer with physiological pH, allowing them to be tested as future MRI contrast agents.

Supplementary Materials: The following supporting information can be downloaded at: https://www.mdpi.com/article/10.3390/cryst14040319/s1, CIFs and check cif reports for compounds **2**–**9**. Table S1. Crystallography data for crystal $\mathbf{[2]^+[O_2CHCF_3]^-}$. Figure S1. Asymmetric unit of crystal $\mathbf{[2]^+[O_2C_2F_3]^-}$ showing 50% probability ellipsoids. Figure S2. Molecular ribbons in crystal of $\mathbf{[2]^+[O_2CF_3]^-}$ showing H-bonds. Figures S3–S8. IR spectra for complexes **4**–**9**. Figure S9. The IR spectra of complexes **4** (green) and **9** (pink) reveal distinct differences, providing confirmation that these two complexes are indeed different dimers. Figure S10. Charge distribution in complex **4** obtained by DFT calculations. Direction of dipole moment is shown with a blue vector. Figures S11–S15. PXRD plots of calculated (Calc) and experimental (EXP) patterns for complexes **4**–**8**. Figure S16. Plots of thermogravimetric analysis for complexes **4**–**9**. Figures S17–S20. The H-1 NMR and Carbon-13 NMR spectra of ligands **2** and **3**.

Author Contributions: Conceptualization: R.C.; methodology: R.C. and T.V.T.; synthesis: Z.Y. and A.P.; X-ray crystal structures investigation: R.C., E.M.N. and Z.Y.; writing—original draft preparation: Z.Y.; writing—review and editing: Z.Y., R.C. and T.V.T. All authors have read and agreed to the published version of the manuscript.

Funding: The authors National Science Foundation, DMR for support PREM project #2122108.

Data Availability Statement: The original contributions presented in the study are included in the article/Supplementary Material, further inquiries can be directed to the corresponding author.

Acknowledgments: We thank New Mexico Highlands University for their technical support.

Conflicts of Interest: The authors declare no conflict of interest.

References

1. Wahsner, J.; Gale, E.M.; Rodríguez-Rodríguez, A.; Caravan, P. Chemistry of MRI Contrast Agents: Current Challenges and New Frontiers. *Chem. Rev.* **2019**, *119*, 957–1057. [CrossRef] [PubMed]
2. Grobner, T. Gadolinium—A specific trigger for the development of nephrogenic fibrosing dermopathy and nephrogenic systemic fibrosis? *Nephrol. Dial. Transplant.* **2006**, *21*, 1104–1108. [CrossRef] [PubMed]
3. Yu-Dong, X.; Ramchandra, P.; Jun, L.; Cong, M.; Zi-Shu, Z.; Shun-Ke, Z. MRI contrast agents: Classification and application (Review). *Int. J. Mol. Med.* **2016**, *38*, 1319–1326.
4. Valerie, C.P.; Matthew, J.A.; Peter, C. Contrast agents for MRI: 30+ years and where are we going? *J. Biol. Inorg. Chem.* **2014**, *19*, 127–131.
5. Kuo, P.H. Gadolinium-Containing MRI Contrast Agents: Important Variations on a Theme for NSF. *J. Am. Coll. Radiol.* **2008**, *5*, 29–35. [CrossRef] [PubMed]
6. Abu-Alfa, A. The Impact of NSF on the Care of Patients With Kidney Disease. *J. Am. Coll. Radiol.* **2008**, *5*, 45–52. [CrossRef] [PubMed]
7. Gallez, B.; Baudelet, C.; Geurts, M. Regional distribution of manganese found in the brain after injection of a single dose of manganese-based contrast agents. *Magn. Reson. Imaging* **1998**, *16*, 1211–1215. [CrossRef] [PubMed]
8. Wang, Y.; Li, W.; Zhou, S.; Kong, D.; Yang, H.; Wu, L. Mn_{12} single-molecule magnet aggregates as magnetic resonance imaging contrast agents. *Chem. Commun.* **2011**, *47*, 3541–3543. [CrossRef]
9. Viswanathan, S.; Kovacs, Z.; Green, K.N.; Ratnakar, S.J.; Sherry, A.D. Alternatives to gadolinium-based metal chelates for magnetic resonance imaging. *Chem. Rev.* **2010**, *110*, 2960–3018. [CrossRef] [PubMed]
10. Zhang, Q.; Gorden, J.D.; Beyers, R.J.; Goldsmith, C.R. Manganese(II)-containing MRI contrast agent employing a neutral and non-macrocyclic ligand. *Inorg. Chem.* **2011**, *50*, 9365–9373. [CrossRef] [PubMed]

11. Dasa, S.; Pargaa, K.; Chakrabortya, I.; Tinocoa, A.D.; Delgadoa, Y.; Lópeza, P.M.; Vegaa, L.F.; Sanakisb, Y.; Ghoshc, S.; Banksond, J.; et al. Magnetic resonance imaging contrast enhancement in vitro and in vivo by octanuclear iron-oxo cluster-based agents. *J. Inorg. Biochem.* **2018**, *186*, 176–186. [CrossRef] [PubMed]
12. Henoumont, C.; Devreux, M.; Laurent, S. Mn-Based MRI Contrast Agents: An Overview. *Molecules* **2023**, *28*, 7275. [CrossRef] [PubMed]
13. Marinescu, M.; Popa, C.-V. Pyridine Compounds with Antimicrobial and Antiviral Activities. *Int. J. Mol. Sci.* **2022**, *23*, 5659. [CrossRef] [PubMed]
14. Zhuang, J.; Ma, S. Recent Development of Pyrimidine-Containing Antimicrobial Agents. *ChemMedChem* **2020**, *15*, 1875–1886. [CrossRef] [PubMed]
15. Hou, W.; Dai, W.; Huang, H.; Liu, S.-L.; Liu, J.; Huang, L.-J.; Huang, X.-H.; Zeng, J.-L.; Gan, Z.-W.; Zhang, Z.-Y.; et al. Pharmacological activity and mechanism of pyrazines. *Eur. J. Med. Chem.* **2023**, *258*, 115544. [CrossRef] [PubMed]
16. Perontsis, S.; Geromichalos, G.D.; Pekou, A.; Hatzidimitriou, A.G.; Pantazaki, A.; Fylaktakidou, K.C.; Psomas, G. Structure and biological evaluation of pyridine-2-carboxamidine copper(II) complex resulting from N′-(4-nitrophenylsulfonyloxy)2-pyridine-carboxamidoxime. *J. Inorg. Biochem.* **2020**, *208*, 111085. [CrossRef] [PubMed]
17. Grineva, O.V.; Zorkii, P.M. Isostructural and Nonisostructural Compounds in Series of Halogenated Organic Crystal Substances. Structure of Hal-Aggregates. *J. Struct. Chem.* **2001**, *42*, 16–23. [CrossRef]
18. Grineva, O.V.; Zorkii, P.M. Aggregation of Halogen Atoms in Crystalline Isomers. *J. Struct. Chem.* **2002**, *43*, 995–1005. [CrossRef]
19. Reddy, C.M.; Kirchner, M.T.; Gundakaram, R.C.; Padmanabhan, K.A.; Desiraju, G.R. Isostructurality, Polymorphism and Mechanical Properties of Some Hexahalogenated Benzenes: The Nature of Halogen···Halogen Interactions. *Chem. Eur. J.* **2006**, *12*, 2222–2234. [CrossRef] [PubMed]
20. Saha, S.; Desiraju, G.R. Crystal Engineering of Hand-Twisted Helical Crystals. *J. Am. Chem. Soc.* **2017**, *139*, 1975–1983. [CrossRef] [PubMed]
21. Fotović, L.; Bedeković, N.; Stilinović, V. Isostructural Halogen Exchange and Halogen Bonds: The Case of N-(4-Halogenobenzyl)-3-halogenopyridinium Halogenides. *Cryst. Growth Des.* **2022**, *22*, 1333–1344. [CrossRef]
22. Kariuki, B.M.; Abdel-Wahab, B.F.; El-Hiti, G.A. Synthesis and Structural Characterization of Isostructural 4-(4-Aryl)-2-(5-(4-fluorophenyl)-3-(1-(4-fluorophenyl)-5-methyl-1H-1,2,3-triazol-4-yl)-4,5-dihydro-1H-pyrazol-1-yl)thiazoles. *Crystals* **2021**, *11*, 795. [CrossRef]
23. Kashina, M.V.; Ivanov, D.M.; Kinzhalov, M.A. The Isocyanide Complexes cis-[$MCl_2(CNC_6H_4$-4-$X)_2$] (M = Pd, Pt; X = Cl, Br) as Tectons in Crystal Engineering Involving Halogen Bonds. *Crystals* **2021**, *11*, 799. [CrossRef]
24. Safin, D.; Tumanov, N.; Leitch, A.A.; Brusso, J.L.; Filinchuk, Y.; Murugesu, M. Elucidating the elusive crystal structure of 2,4,6-tris(2-pyrimidyl)-1,3,5-triazine (TPymT) Through X-ray Powder Diffraction. *CrystEngComm* **2015**, *17*, 2190–2195. [CrossRef]
25. Sheldrick, G.M. SHELXT—Integrated space-group and crystal-structure determination. *Acta Cryst.* **2015**, *C71*, 3–8. [CrossRef] [PubMed]
26. Frisch, M.J.; Trucks, G.W.; Schlegel, H.B.; Scuseria, G.E.; Robb, M.A.; Cheeseman, J.R.; Scalmani, G.; Barone, V.; Petersson, G.A.; Nakatsuji, H.; et al. *Gaussian 16, Revision C.01*; Gaussian, Inc.: Wallingford, UK, 2016.
27. Michalczyk, M.; Piec, K.; Zierkiewicz, W.; Ejfler, J.; Łukasz, J. Possible coordination modes of copper(II) atom in model silsesquioxanes complexes at various pH conditions: DFT study. *Chem. Phys. Lett.* **2021**, *778*, 138739. [CrossRef]
28. Batsanov, S.S. Van der Waals Radii of Elements. *Inorg. Mater.* **2001**, *37*, 871–885. [CrossRef]
29. Chilton, N.F.; Anderson, R.P.; Turner, L.D.; Soncini, A.; Murray, K.S.J. PHI: A powerful new program for the analysis of anisotropic monomeric and exchange-coupled polynuclear d- and f-block complexes. *Comput. Chem.* **2013**, *34*, 1164–1175. [CrossRef] [PubMed]
30. Reinen, D. Cu^{2+}, a Chameleon in Coordination Chemistry. *Comments Inorg. Chem.* **2006**, *2*, 227–246. [CrossRef]
31. Wertz, J.E.; Bolton, J.R. Basic Principles of Electron Spin Resonance. In *Electron Spin Resonance*; Springer: Dordrecht, The Netherlands, 1986; 497p.